

Electronic States of Magnetic Quantum Dots

Ramin M. Abolfath^{1,2,3}, Pawel Hawrylak², and Igor Žutić¹

¹ *Department of Physics, State University of New York at Buffalo, Buffalo, New York 14260, USA*

² *Institute for Microstructural Sciences, National Research Council of Canada, Ottawa, K1A 0R6, Canada*

³ *Department of Radiation Oncology, University of Texas Southwestern Medical Center, Dallas, Texas 75390, USA*

We study quantum states of electrons in magnetically doped quantum dots as a function of exchange coupling between electron and impurity spins, the strength of Coulomb interaction, confining potential, and the number of electrons. The magnetic phase diagram of quantum dots, doped with a large number of magnetic Mn impurities, can be described by the energy gap in the spectrum of electrons and the mean field electron-Mn exchange coupling. A competition between these two parameters leads to a transition between spin-unpolarized and spin-polarized states, in the absence of applied magnetic field. Tuning the energy gap by electrostatic control of nonparabolicity of the confining potential can enable control of magnetization even at the fixed number of electrons. We illustrate our findings by directly comparing Mn-doped quantum dots with parabolic and Gaussian confining potential.

Recent experimental [1, 2, 3, 4, 5, 6, 7, 8, 9] and theoretical [10, 11, 12, 13, 14, 15] studies reveal that semiconductor quantum dots (QDs) [16, 17] are desirable for tailoring magnetism which persists at much high temperatures than in their bulk counterparts [18]. These nanoscale realizations of dilute magnetic semiconductors (DMS) [19] may be suitable for a versatile control of spin and magnetism with potential applications in information storage technology and spintronics [20]. An important property of the carrier-mediated ferromagnetism in bulk-like DMS is the optical and electrical control of the magnetic ordering by changing the number of carriers [21, 22, 23]. However, because of the strong interplay between quantum confinement and the many-body electron-electron (e-e) Coulomb interactions in QDs, it may be possible to achieve and control the magnetic ordering of carrier spin and magnetic impurities, with a fixed number of carriers [15].

In this paper, we present a theoretical analysis to describe the quantum states of the electrons confined in II-VI quantum dots doped with Mn. In (II,Mn)VI materials, Mn does not change the number of electrons (N) because it is isoelectronic with group-II elements. In QDs, however, additional carriers are controlled by either chemical doping or by an external electrostatic potential applied to the metallic gates. Even for a small number of interacting electrons, the study of QDs doped with large numbers of Mn (> 10) becomes computationally inaccessible to exact diagonalization techniques [14, 15]. For this reason we employ here a mean field theory of magnetic QDs in which Mn acts like an external magnetic field and the weak coupling between electrons and magnetic impurities can be described as spin-spin exchange interaction [15]. Because electrons are confined in all three dimensions in nanometer-sized QDs, we anticipate strong electron-electron (e-e) Coulomb interaction. We use a finite temperature local spin density approximation (LSDA) [24] to incorporate e-e Coulomb interaction in this work.

The wave function of electrons in QDs can be expanded in terms of its planar $\psi_{i\sigma}(\vec{\rho})$ with $\vec{\rho} \equiv (x, y)$, and subband wave function $\xi(z)$. The effective two-dimensional (2D) Kohn-Sham (KS) equations $H\psi_{i\sigma}(\vec{\rho}) = \epsilon_{i\sigma}\psi_{i\sigma}(\vec{\rho})$, in LSDA can be obtained by integrating $\xi(z)$ [25], assuming that the first subband is filled. Here $\epsilon_{i\sigma}$ are the KS eigenenergies, $\sigma = +1$ and -1 for spin up (\uparrow) and down (\downarrow), and H is the Kohn-Sham Hamiltonian which can be expressed as

$$H = \frac{-\hbar^2}{2m^*} \nabla_{\rho}^2 + V_{QD} + \gamma V_H + \gamma V_{XC}^{\sigma} - \frac{\sigma}{2} h_{sd}(\vec{\rho}). \quad (1)$$

where \hbar is the Planck constant, m^* is the electron effective mass, and $V_{QD} = V_0 \exp(-\rho^2/\delta^2)$ is the 2D Gaussian confining potential of the quantum dot (1D parabolic confinement is chosen along the z -axis). In Eq.(1), V_H and V_{XC}^{σ} are Hartree and spin dependent exchange-correlation potentials [24], while γ accounts for reduction of Coulomb strength due to screening effects of the gate electrodes [27] and

$$h_{sd}(\vec{\rho}) = J_{em} \int dz |\xi(z)|^2 B_M \left(\frac{Mb(\vec{\rho}, z)}{k_B T} \right). \quad (2)$$

$J_{em} = J_{sd} n_m M$ is the e-Mn exchange coupling, J_{sd} is the exchange coupling between electron and single Mn, n_m is the spatial-averaged density of Mn, and $M = 5/2$ is the spin of Mn. $B_M(x)$ is the Brillouin function [26] in which the argument x contains k_B the Boltzmann constant, T the absolute temperature, and

$$b(\vec{\rho}, z) = -J_{\text{eff}}^{AF} \langle M_z(\vec{\rho}, z) \rangle + \frac{J_{sd}}{2} [n_{\uparrow}(\vec{\rho}, z) - n_{\downarrow}(\vec{\rho}, z)], \quad (3)$$

the effective field seen by the Mn [15]. The first term in $b(\vec{\rho}, z)$ describes the mean field of the direct Mn-Mn antiferromagnetic coupling [12], with

$$\langle M_z(\vec{\rho}, z) \rangle = M B_M \left(\frac{Mb(\vec{\rho}, z)}{k_B T} \right), \quad (4)$$

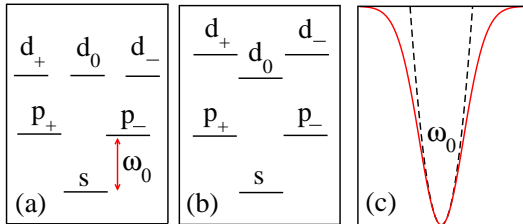


FIG. 1: The schematic single particle levels of a 2D parabolic (a) and 2D Gaussian (b) confining potentials corresponding to dashed and bold lines in (c).

and

$$n_{\sigma}(\vec{\rho}, z) = \sum_i |\psi_{i\sigma}(\vec{\rho})|^2 |\xi(z)|^2 f(\epsilon_{i\sigma}), \quad (5)$$

is the spin-resolved electron density, $f(\epsilon) = 1/\{\exp[(\epsilon - \mu)/k_B T] + 1\}$ is the Fermi function, and μ is the temperature-dependent chemical potential, and is the self-consistent solution of $N = \sum_{i,\sigma} f(\epsilon_{i\sigma})$ which ensures that $N = N_{\uparrow} + N_{\downarrow}$ is an integer number.

To obtain solutions of Eqs. (1)-(5), we consider (Cd,Mn)Te QD with $V_0 = -128$ meV, and $\delta = 15.9$ nm, a perpendicular width of 1 nm, $J_{sd} = 0.015$ eV nm³, $n_m = 0$, 0.025, 0.1 nm⁻³, corresponding to the approximate number of Mn, $N_{\text{Mn}} = 0$, 45, 180, $J_{em} = 0$, 0.94, 3.75 meV, and $J_{\text{eff}}^{AF} = 0$, 0.005, 0.02 meV, respectively. For CdTe, considered here, $a_B^* = 5.29$ nm, and $Ry^* = 12.8$ meV are the effective Bohr radius and Rydberg energy, while the additional material parameters are $m^* = 0.106$, and $\epsilon = 10.6$ [15].

The shell structure of the 2D parabolic (a) and 2D Gaussian (b) potentials are shown in Fig. 1. The corresponding confining potentials are shown in Fig. 1(c) where the dashed and bold lines represent the 2D parabolic and 2D Gaussian potentials. The distinction between parabolic and Gaussian potentials can be experimentally resolved by photo-emission spectroscopy or transport measurements of single particle states in external magnetic field [16, 17]. The energy gap between s -, p -, and d -orbitals is characterized by ω_0 . For a 2D Gaussian potential, the characteristic energy associated with the perpendicular confinement, ω_0 , is calculated by expanding V_{QD} in the vicinity of the minimum which yields $V_{QD} = V_0 + m^* \omega_0^2 \rho^2 / 2 + \dots$, with the strength $\omega_0 = \sqrt{2|V_0|/m^*}/\delta$. Because of the circular symmetry of the Gaussian potential, the z -component of the angular momentum l_z is a good quantum number. As a result of the geometrical symmetry of the confining potential, the states in p -shell with $l_z = \pm 1$ are degenerate. In contrast to the 2D parabolic potential [16, 17], where the dynamical symmetry of the confining potential implies

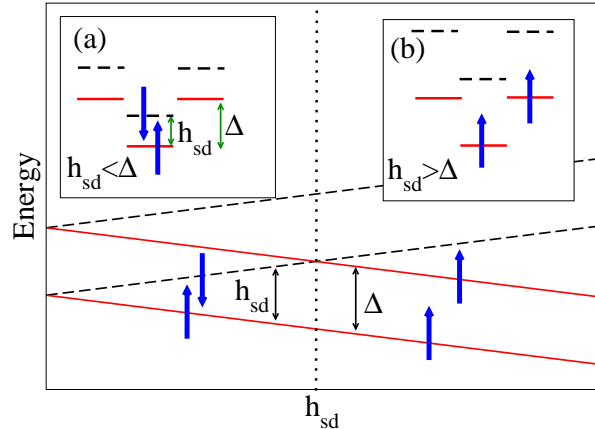


FIG. 2: Single particle levels of the d -shell as a function of effective Zeeman energy h_{sd} . The insets (a) and (b) schematically show the ground state of $N = 8$ depending on the relative magnitude of h_{sd} and the single particle energy gap Δ . At $\Delta = h_{sd}$ (shown by dashed line) a transition from anti-ferromagnetic to ferromagnetic state is predicted. Filled and dashed lines represent the single particle eigenenergies of the electrons with spin up and down.

occurrence of accidental degeneracies of the single particle levels with different $|l_z|$, the single particle levels in d -shell are not completely degenerate. Degenerate levels d_+ and d_- are separated by an energy gap (1.5 meV) from the d_0 -level, where the indices $\pm, 0$ refer to angular momentum $l_z = \pm 1, 0$. We note that the ordering of the single particle s -, p -, and d -eigenenergies in the Gaussian potential are similar to the ordering of the first few single particle eigenenergies in a square potential.

In the absence of direct antiferromagnetic coupling between Mn, and e-e Coulomb interaction, an identification of the magnetic states of the QDs based on the present mean field theory can be expressed in terms of two energy scales: the single particle energy gap Δ , and the effective e-Mn exchange coupling J_{em} . The former is the energy difference between the highest occupied molecular orbital (HOMO) and the lowest unoccupied molecular orbital (LUMO). It is a function of the number and spin of electrons, and the geometrical and dynamical symmetries of the QD confining potential. Therefore Δ , which depends on the quantum confinement, can be tuned and controlled by the electric voltage applied to the metallic gates. On the other hand, J_{em} , the strength of the effective Zeeman energy, $h_{sd} \equiv \langle h_{sd}(\vec{\rho}) \rangle$, which polarizes spin of electrons, is independent of the quantum confinement. Thus the magnetic phase diagram of the QDs can be effectively described in terms of Δ , and J_{em} . In the absence of magnetic field we can then distinguish between spin-polarized and spin-unpolarized states in QDs,

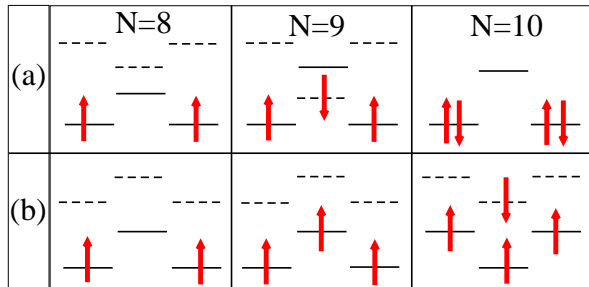


FIG. 3: Spin up (bold lines), and spin down (dashed lines) show Kohn-Sham eigenstates of $N = 8, 9, 10$ electrons in d -shell in 2D Gaussian confining potential with $V_0 = -128$ meV, $\delta = 15.9$ nm, $n_m = 0$ (a), and $n_m = 0.1$ nm $^{-3}$ (b). For clarity, s - and p -levels are not shown.

conventionally also referred to as the ferromagnetic (FM) and antiferromagnetic (AFM) states [12, 13, 14]. For example, the ground state of the electrons exhibits FM ordering if $J_{em} > \Delta$. The dependence of the single particle eigenenergies of the d -shell with $N = 8$ on h_{sd} is shown in Fig. 2. At $h_{sd} = 0$ the valence electrons with spin up and down occupy single particle level d_0 , following the Pauli exclusion principle, and the ground state of $N = 8$ exhibits AFM ordering with $N_\uparrow = N_\downarrow = 4$. With increasing h_{sd} the gap between spin up and spin down opens up. At $h_{sd} = \Delta = 1.5$ meV, where $\Delta = E_{d_+(d_-)} - E_{d_0}$, the first spin flip occurs. Because of well separated p - and d -orbitals the second spin flip occurs at much higher energies as $h_{sd} = \omega_0 \approx 7J_{em}$.

In LSDA, electrons are replaced by independent quasi-particles (electrons dressed by e-e interaction), where KS eigenenergies are the energy levels of the quasi-particles. In this picture, e-e interaction rearrange the structure of quantized levels, and affects the shell structure of the QDs. In this limit, the quasi-particle gap Δ^* (renormalized Δ) is the energy difference between HOMO and LUMO of the KS eigenenergies. It is an appropriate parameter, which can supersede the single particle gap Δ in identification of the magnetic states of the QDs.

The KS levels in the d -shell of the 2D Gaussian potential with $n_m = 0$ and $N = 8, 9, 10$ are shown in Fig. 3(a). Because of circular symmetry of the confining potential, the energy levels of d_+ and d_- are degenerate. The energy of d_0 which was lower than d_+ and d_- due to the nonparabolicity of the Gaussian potential, increases by e-e Coulomb interaction, such that it becomes the highest energy level in d -shell, and Δ^* changes sign. In contrast to non-interacting electrons, the ordering of the KS levels in s -, p -, and d -shells is closer to the one in circular potential than in the square potential. In the absence of magnetic impurities, as it is shown in Fig. 3(a), $N = 8$

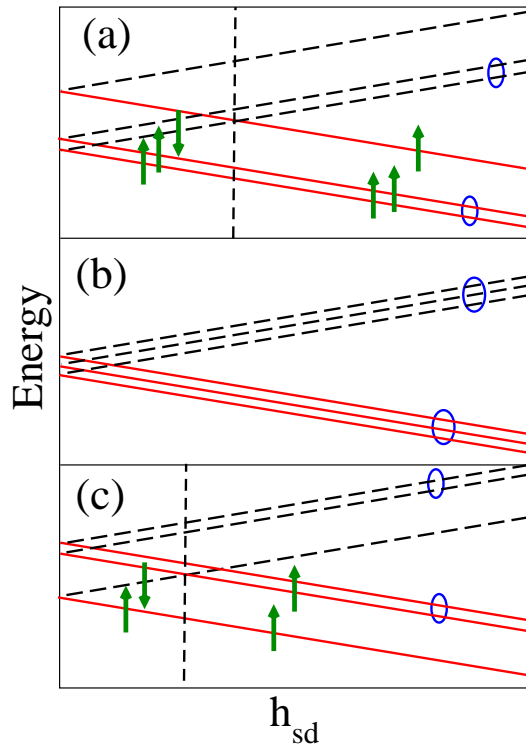


FIG. 4: Energy of quantized states in 2D Gaussian confining potential with spin up (bold lines) and spin down (dashed lines) in d -shell as a function of effective Zeeman energy h_{sd} corresponding to $\Delta^* < 0$ (a), $\Delta^* = 0$ (b), and $\Delta^* > 0$ (c). Energy levels marked with circles are degenerate and shifted with respect to each other for enhanced visibility. The first spin flip occurs if $\Delta^* < 0$, $N = 9$ (a), and $\Delta^* > 0$, $N = 8$ (c). No spin flip occurs if $\Delta^* = 0$ (b).

forms a half-filled shell with $s_z = 1$, and the electron polarization $P = 2/8$, and $N = 9$ shows an open shell with $s_z = 1/2$, and $P = 1/9$. Because of d -shell overturning, $N = 10$ forms a closed shell with $s_z = 0$, and $P = 0/10$. Here the energy difference between the KS eigenenergies of the electrons with spin up and down is zero, and $\Delta^* \approx 0.6$ meV ($< J_{em}$). With increasing e-Mn coupling to $J_{em} = 3.75$ meV, corresponding to 5% doping, and within a range that spin polarization happens only in d -shell, we find no magnetic transition for $N = 8$, since it was already fully polarized due to the spin Hund's rule, whereas for $N = 9$ and $N = 10$ we find transitions to $s = 3/2$ and $s = 1$ respectively. The evolution of quantized energies as a function of effective Zeeman energy and Δ^* is shown in Fig. 4. For examples $\Delta^* < 0$ corresponds to d -levels of the 2D Gaussian potential with $\gamma = 1$, whereas $\Delta^* = 0$ (b), and $\Delta^* > 0$ (c) correspond to d -levels in the 2D parabolic and 2D Gaussian potentials with $\gamma = 0$ ($\Delta^* = \Delta$).

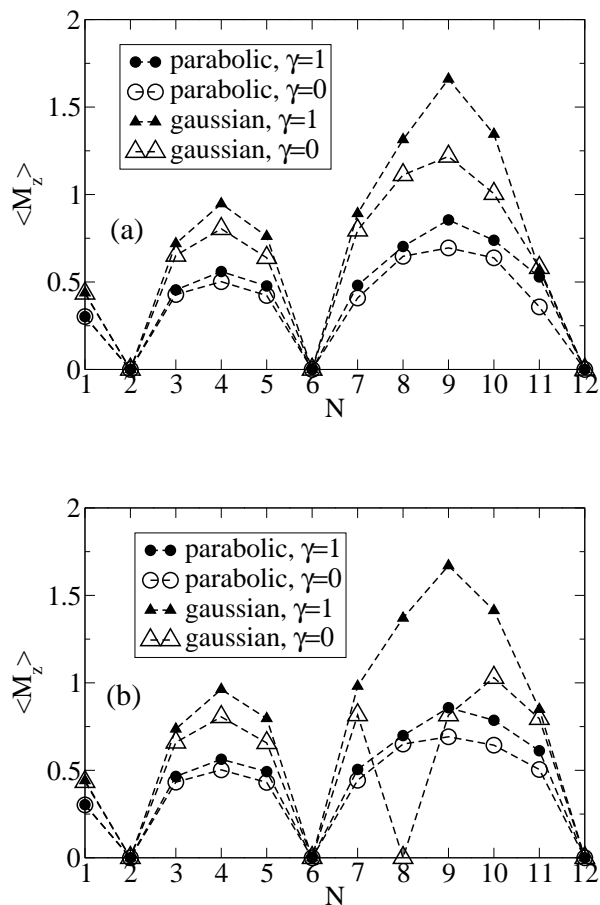


FIG. 5: The averaged magnetization per unit area $\langle M_z \rangle$ as a function of number of electrons N at $T = 1K$ and Mn-density $n_m = 0.1 \text{ nm}^{-3}$ (a), and $n_m = 0.025 \text{ nm}^{-3}$ (b) for non-interacting ($\gamma = 0$, empty triangles) and interacting ($\gamma = 1$, filled triangles) electrons. At $N = 8$, $n_m = 0.025 \text{ nm}^{-3}$, in 2D Gaussian confining potential the ground state of the QD switches between ferromagnetic and antiferromagnetic states by e-e Coulomb interaction.

We next turn to calculate the spatially-averaged Mn-magnetization per unit area A , $\langle M_z \rangle = \frac{1}{A} \int d^2\rho \langle M_z(\vec{\rho}) \rangle$ for the 2D parabolic and 2D Gaussian potentials as a function of N for zero ($\gamma = 0$), and full ($\gamma = 1$) e-e Coulomb interaction in Fig. 5. This calculation illustrates how deviation from nonparabolicity of the confining potential may lead to changes in the magnetic properties of QDs. Many qualitative features indeed coincide for both of the confinements.

A comparison in Fig. 5(a) for $n_m = 0.1 \text{ nm}^{-3}$, confirms that there is similarity in magnetization for both Gaussian and parabolic confinements. Here $J_{em} > \Delta^*$ (Δ) for $\gamma = 1$ (0) and we consider all the electron numbers up to a full d -shell ($N \leq 12$). However, as we show in Fig. 5(b) a nonparabolic confinement can introduce additional magnetic transitions in quantum dots. Here $n_m = 0.025 \text{ nm}^{-3}$ corresponds to a magnetic doping of

1.25 %. At $N = 8$ and $\gamma = 0$ in the 2D Gaussian potential, we find that $J_{em} < \Delta$ and a transition to the AFM state. In contrast, at $\gamma = 1$, we find $J_{em} > \Delta^*$, and thus the FM state is stable.

Our findings illustrate the importance of Coulomb interactions and quantum confinement for the magnetic ordering of carrier spin and magnetic impurities in (II,Mn)VI quantum dots. We show that with electrostatic control of nonparabolicity of the confining potential, it is possible to control the magnetization of QDs even with a fixed number of electrons. While the choice of 2D Gaussian confinement is a convenient form to parameterize nonparabolic effects, other deviations from the parabolic confinement could also influence the magnetic ordering in quantum dots [28].

This work is supported by the US ONR, NSF-ECCS CAREER, the NRC HPC project, CIAR, the CCR at SUNY Buffalo, and the Center for Nanophase Materials Sciences, sponsored at ORNL by the Division of Scientific User Facilities, US DOE.

-
- [1] S. Mackowski, T. Gurung, T. A. Nguyen, H. E. Jackson, and L. M. Smith, G. Karczewski and J. Kossut, Appl. Phys. Lett. **84**, 3337 (2004).
 - [2] C. Gould, A. Slobodskyy, T. Slobodskyy, P. Grabs, D. Supp, P. Hawrylak, F. Qu, G. Schmidt, L.W. Molenkamp, Phys. Rev. Lett. **97**, 017202 (2006). Quantum Dot
 - [3] L. Besombes, Y. Leger, L. Maingault, D. Ferrand, and H. Mariette, Phys. Rev. Lett. **93**, 207403 (2004); Phys. Rev. B **71**, 161307 (2005).
 - [4] Y. Léger, L. Besombes, J. Fernández-Rossier, L. Maingault, and H. Mariette, Phys. Rev. Lett. **97**, 107401 (2006); Y. Léger, L. Besombes, L. Maingault, D. Ferrand, and H. Mariette, Phys. Rev. Lett. **95**, 047403 (2005).
 - [5] S. Chakrabarti, M. A. Holub, P. Bhattacharya, T. D. Mishima, M. B. Santos, M. B. Johnson, D. A. Blom, Nano Lett. **5**, 209 (2005); M. Holub, S. Chakrabarti, S. Fathpour, P. Bhattacharya, Y. Lei, and S. Gosh, Appl. Phys. Lett. **85**, 973 (2004).
 - [6] P. Wojnar, J. Suffczynski, K. Kowalik, A. Golnik, G. Karczewski, and J. Kossut, Phys. Rev. B **75**, 155301 (2007).
 - [7] P. I. Archer, S. A. Santangelo, and D. R. Gamelin, Nano Lett. **7**, 1037 (2007).
 - [8] W. K. Liu, K. M. Whitaker, K. R. Kittilstved, and D. R. Gamelin, J. Am. Chem. Soc. **128**, 3911 (2006).
 - [9] Y.-H. Zheng, J.-H. Zhao, J.-F. Bi, W.-Z. Wang, Y. Ji, X.-G. Wu, and J.-B. Xia, Chin. Phys. Lett. **24**, 2118 (2007).
 - [10] P. Hawrylak, M. Grabowski and J.J. Quinn, Phys. Rev. B **44**, 13082 (1991).
 - [11] A. K. Bhattacharjee and C. Benoit à la Guillaume, Phys. Rev. B **55**, 10613 (1997).
 - [12] J. Fernández-Rossier and L. Brey, Phys. Rev. Lett. **93**, 117201 (2004). J. Fernández-Rossier, Phys. Rev. B **73**, 045301 (2006).
 - [13] A. O. Govorov, Phys. Rev. B **72**, 075358 (2005); Phys.

- Rev. B **72**, 075359 (2005).
- [14] F. Qu and P. Hawrylak, Phys. Rev. Lett. **95**, 217206 (2005); Phys. Rev. Lett. **96**, 157201 (2006).
- [15] R. M. Abolfath, P. Hawrylak, and I. Žutić, Phys. Rev. Lett. **98**, 207203 (2007).
- [16] L. Jacak, P. Hawrylak, and A. Wojs, *Quantum Dots* (Springer, Berlin, 1998); D. Bimberg, M. Grundmann, N. N. Ledentsov, *Quantum Dot Heterostructures*, John Wiley & Sons (Chichester 1999); E. Borovitskaya and M. S. Shur (Eds.), *Quantum Dots* (World Scientific, New Jersey, 2002).
- [17] S. M. Reimann and M. Manninen, Rev. Mod. Phys. **74**, 1283 (2002), and the references therein.
- [18] T. Dietl, A. Haury and Y. Merle d'Aubigné, Phys. Rev. B **55**, R3347 (1997).
- [19] J. K. Furdyna, J. Appl. Phys. **64**, R29 (1988); T. Dietl, H. Ohno and F. Matsukura, Phys. Rev. B **63** 195205 (2001); M. Abolfath, T. Jungwirth, J. Brum, and A. H. MacDonald, Phys. Rev. B **63**, 054418 (2001); S. C. Erwin and I. Žutić, Nature Mater. **3**, 410 (2004).
- [20] I. Žutić, J. Fabian, and S. Das Sarma, Rev. Mod. Phys. **76**, 323 (2004).
- [21] S. Koshihara, A. Oiwa, M. Hirasawa, S. Katsumoto, Y. Iye, C. Urano, H. Takagi, and H. Munekata, Phys. Rev. Lett. **78**, 4617 (1997).
- [22] H. Ohno, D. Chiba, F. Matsukura, T. Omiya, E. Abe, T. Dietl, Y. Ohno, K. Ohtani, Nature (London) **408**, 944 (2000); D. Chiba, M. Yamanouchi, F. Matsukura, and H. Ohno, Science **301**, 943 (2003).
- [23] H. Boukari, P. Kossacki, M. Bertolini, D. Ferrand, J. Cibert, S. Tatarenko, A. Wasiela, J. A. Gaj, and T. Dietl, Phys. Rev. Lett. **88**, 207204 (2002).
- [24] C. Dharma-wardana, and F. Perrot in *Density Functional Theory*, Edited by E. K. U. Gross, and R.M. Dreizler (Plenum Press, New York, 1995).
- [25] X. Xia and J. J. Quinn, Phys. Rev. B **46**, 12530 (1992).
- [26] N. W. Ashcroft and N. D. Mermin, *Solid State Physics*, (Saunders, Philadelphia, 1976).
- [27] N. A. Bruce and P. A. Maksym, Phys. Rev. B **61**, 4718 (2000).
- [28] Ramin M. Abolfath, Andre Petukhov, Igor Zutic, cond-mat/0707.2805.